










RESEARCH ARTICLE | MAY 15 2024

Ionic control of magnetism in all-solid-state CoO_x /yttria-stabilized zirconia heterostructures

Zheng Ma ; Zhengwei Tan ; Alberto Quintana ; Irena Spasojevic ; Nicolau López-Pintó ; Florencio Sánchez ; Ignasi Fina ; Javier Herrero-Martín ; Enric Menéndez ; Jordi Sort 

 Check for updates

Appl. Phys. Lett. 124, 202404 (2024)

<https://doi.org/10.1063/5.0206743>

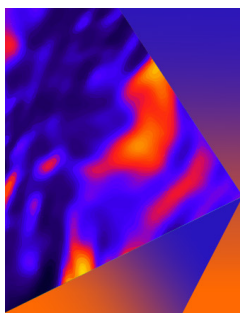


View
Online



Export
Citation

04 July 2024 16:08:55



Applied Physics Letters

Special Topic: Mid and Long Wavelength Infrared Photonics, Materials, and Devices

Submit Today

 AIP
Publishing

 AIP
Publishing

Ionic control of magnetism in all-solid-state CoO_x /yttria-stabilized zirconia heterostructures

Cite as: Appl. Phys. Lett. **124**, 202404 (2024); doi: 10.1063/5.0206743

Submitted: 4 March 2024 · Accepted: 7 May 2024 ·

Published Online: 15 May 2024



View Online



Export Citation



CrossMark

Zheng Ma,^{1,a)} Zhengwei Tan,¹ Alberto Quintana,² Irena Spasojevic,¹ Nicolau López-Pintó,¹ Florencio Sánchez,² Ignasi Fina,² Javier Herrero-Martín,³ Enric Menéndez,¹ and Jordi Sort^{1,4,a)}

AFFILIATIONS

¹Departament de Física, Universitat Autònoma de Barcelona, Cerdanyola del Vallès 08193, Spain

²Institut de Ciència de Materials de Barcelona, ICMAB-CSIC, Campus UAB, 08193 Bellaterra, Barcelona, Spain

³ALBA Synchrotron Light Facility, 08290 Cerdanyola del Vallès, Barcelona, Spain

⁴Institució Catalana de Recerca i Estudis Avançats (ICREA), Pg. Lluís Companys 23, Barcelona 08010, Spain

^{a)} Authors to whom correspondence should be addressed: ma.zheng@uab.cat and jordi.sort@uab.cat

ABSTRACT

Magneto-ionic gating, a procedure that enables the modulation of materials' magnetic properties by voltage-driven ion motion, offers alternative perspectives for emerging low-power magnetic storage and spintronic applications. Most previous studies in all-solid-state magneto-ionic systems have focused on the control of interfacial magnetism of ultrathin (i.e., 1–3 nm) magnetic films, taking advantage of an adjacent ionic conducting oxide, usually GdO_x or HfO_x , that transports functional ionic species (e.g., H^+ or O^{2-}). Here, we report on room-temperature OFF–ON ferromagnetism by solid-state magneto-ionics in relatively thick (25 nm) patterned CoO_x films grown on an yttria-stabilized zirconia (YSZ) layer, which acts as a dielectric to hold electric field and as an O^{2-} ion reservoir. Upon negatively biasing, O^{2-} ions from the CoO_x tend to migrate toward the YSZ gate electrode, leading to the gradual generation of magnetization (i.e., OFF-to-ON switching of a ferromagnetic state). X-ray absorption and magnetic circular dichroism studies reveal subtle changes in the electronic/chemical characteristics, responsible for the induced magnetoelectric effects in such all-oxide heterostructures. Recovery of the initial (virtually non-magnetic) state is achieved by application of a positive voltage. The study may guide future development of all-solid-state low-power CMOS-compatible magneto-ionic devices.

© 2024 Author(s). All article content, except where otherwise noted, is licensed under a Creative Commons Attribution (CC BY) license (<https://creativecommons.org/licenses/by/4.0/>). <https://doi.org/10.1063/5.0206743>

The control of magnetism by means of voltage-driven ion motion, i.e., magneto-ionics, is emerging as an important enabler for advanced next-generation energy-efficient magnetic memory and computing technologies. Magneto-ionics can cause a large nonvolatile modulation of a variety of magnetic properties, such as coercivity, anisotropy, magnetization, exchange bias, domain wall motion, or skyrmion density, even inducing transitions between paramagnetic and ferromagnetic states in some cases.^{1–6} Most magneto-ionic studies have focused on the effects of triggering the motion of ions from an ion reservoir (e.g., HfO_2 ,⁷ GdO_x ,⁸ and liquid electrolyte with Li^+ in dissolution⁹) to an adjacent target magneto-ionic film (typically, a ferromagnetic metal or ferrimagnetic transition metal oxide). In addition, we have shown during the last few years, that it is also possible to induce the appearance of ferromagnetic properties starting from initially paramagnetic films that contain the mobile ions (e.g., O^{2-} or N^{3-}) in their structure.^{10–13} However, so far, structural ion approaches have involved immersing the films of interest in a liquid electrolyte which, upon voltage application, acts as an

ion reservoir. The use of liquid electrolytes is advantageous for fundamental studies since it enables the generation of large electric fields through very narrow electric double layers. However, liquid electrolytes are often detrimental for practical applications. Shifting paradigm to all-solid magneto-ionic structures is appealing but often challenging because of the occurrence of pinholes that preclude application of sufficiently high electric fields to trigger ion motion.

However, it is known that yttria-stabilized zirconia (YSZ) is widely explored as an efficient oxygen ion conductor in the context of solid oxide fuel cells and oxygen sensors, thanks to the high oxygen vacancy concentration introduced in the ZrO_2 crystal structure upon addition of an optimal amount of Y_2O_3 (thereby providing high O^{2-} ion conductivity).^{14–16} Recently, a superior hydrogen magneto-ionic response was demonstrated in an ultrathin-layer stack YSZ/Co/Pt system (YSZ as a proton-conducting oxide) by electrolyzing atmospheric water (humidity), giving rise to proton-induced control of interfacial magnetic anisotropy.¹⁷

Here, we demonstrate the viability of voltage-controlled generation of ferromagnetism from paramagnetic oxides at room temperature by motion of oxygen ions in Pt (top electrode)/CoO_x patterned films grown on a YSZ layer, which acts as a dielectric to hold electric field and as an oxygen ion reservoir. YSZ is grown atop a conducting Si substrate, that serves as bottom electrode (all-solid-state configuration). The main magnetic parameters of the induced ferromagnetic behaviors (coercivity, saturation magnetization, and squareness ratio) are found to scale with the gating time in an analogic manner. A threshold voltage to induce all these effects is also noted. These features suggest that this approach may find applications in solid-state magneto-ionic synaptic applications.^{18–20}

YSZ dielectric oxide films (60 nm in thickness) were grown by pulsed laser deposition (PLD) on n-doped (with resistivity in the range 0.01–0.015 Ω cm) Si(001) wafers. The Si(001) crystal acts as substrate and also as a bottom electrode during electrolyte gating. During the PLD process at high temperature ($T = 800^\circ\text{C}$), the YSZ films grow epitaxially onto Si after local reduction of the native SiO_x.^{21–23} The (001)-oriented growth of YSZ is confirmed by x-ray diffraction θ - 2θ scans (see [supplementary material S1](#)). Subsequently, an array of disks of $\approx 100\ \mu\text{m}$ in diameter, comprising cobalt oxide (CoO_x) and a Pt

capping layer, were deposited at room temperature by magnetron sputtering, on the YSZ film using shadow masks. The oxide was deposited by reactive sputtering under a partial pressure of 3×10^{-3} Torr. The thicknesses of CoO_x and Pt layers are 25 and 5 nm, respectively. Co $L_{2,3}$ x-ray absorption (XAS) study on the as-grown sample reveals a predominant Co²⁺ oxidation state with minor Co³⁺ contribution (see [supplementary material S2](#)). For electrical actuation of the CoO_x/YSZ heterostructures, negative bias voltages, V_G , were applied to the Pt top electrode at room temperature through a probe tip connected to a TFAAnalyser2000 platform (aixACCT Systems GmbH), while grounding the bottom electrode Si, as shown in [Fig. 1\(a\)](#). Gate voltages up to $-7\ \text{V}$ were applied to prevent partial breakdown of the devices. *Ex situ* magnetometry measurements using a longitudinal magneto-optical Kerr effect (MOKE) were used to record the in-plane hysteresis loops of the disks. Furthermore, XAS and x-ray magnetic circular dichroism (XMCD) analyses were used to probe the local electronic structure evolution. To favor the depth sensitivity of the measurements, the XAS signal in fluorescence yield mode was collected at the BL29 BOREAS beamline of the ALBA Synchrotron Light Facility, Spain.²⁴ All the characterizations were conducted at room temperature.

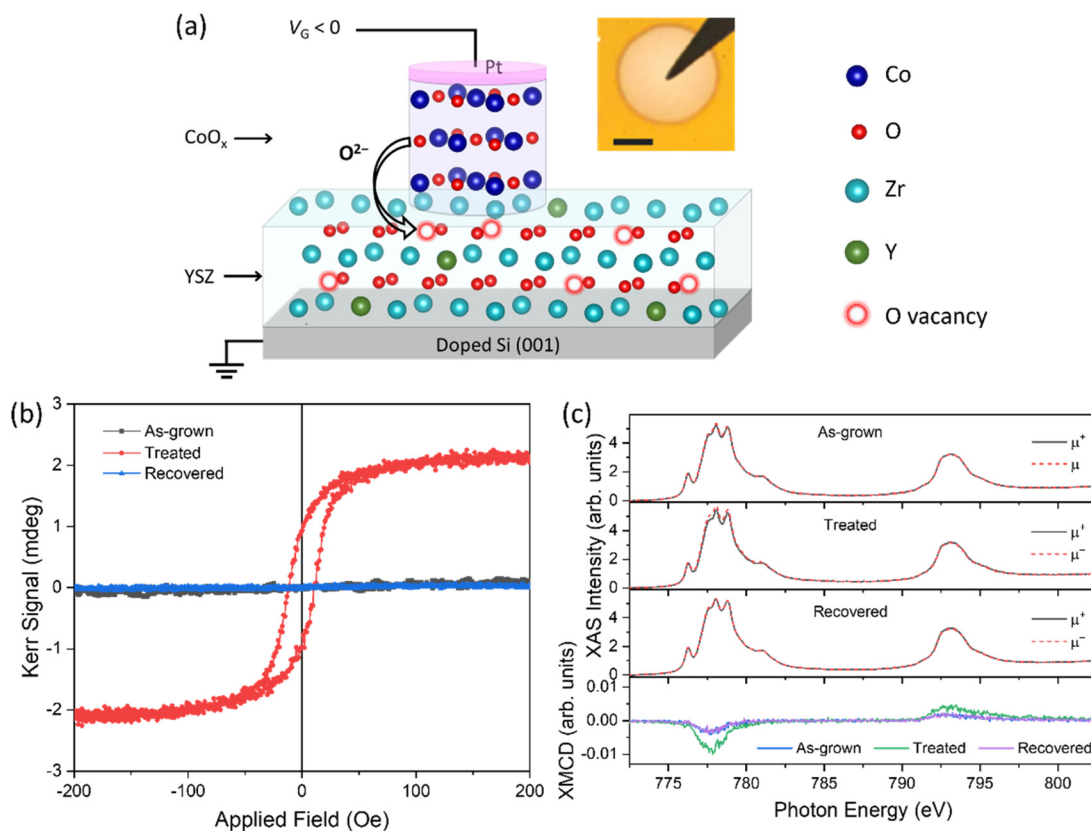


FIG. 1. (a) Sketch of the CoO_x/YSZ devices and the oxygen ion migration mechanism in the heterostructures upon electric field actuation. Under negative V_G , part of the oxygen ions bonded to Co are injected into the YSZ electrolyte lattice, which is rich in oxygen vacancies. The upper right inset shows the optical micrograph of the fabricated device with bias voltages, V_G , applied to the Pt top electrode through a probe tip. Scale bar: $50\ \mu\text{m}$. (b) Hysteresis loops of the CoO_x/YSZ heterostructures in the as-grown state (in black), after applying a $V_G = -5\ \text{V}$ for 10 s (treated state, in red), and after a final biasing using opposite voltage ($+5\ \text{V}$) for 80 s (recovered state, in blue). (c) Co $L_{2,3}$ -edge XAS and XMCD spectra for the as-grown, treated, and recovered CoO_x/YSZ structures. Absorption spectra of right (μ^+) and left (μ^-) circularly polarized x rays are depicted in dashed red and black solid lines, respectively.

Figure 1(b) shows the in-plane hysteresis loops recorded via a longitudinal magneto-optical Kerr effect (MOKE) for the as-grown, treated ($V_G = -5$ V for 10 s), and recovered ($V_G = -5$ V for 10 s followed by $V_G = +5$ V for 80 s) samples. While virtually no MOKE signal is observed in the pristine state, in agreement with the paramagnetic character of CoO_x at room temperature (i.e., OFF ferromagnetism), a clear hysteresis loop develops (i.e., ON ferromagnetism) after actuation using negative voltage. The appearance of hysteresis behavior is related to the partial reduction of CoO_x to Co due to the migration of oxygen ions toward the YSZ layer as a response of the negative bias application. It is known that ion-conducting YSZ thin films typically work effectively above $\sim 450^\circ\text{C}$ in solid oxide fuel cells.^{25,26} When YSZ is used as a reservoir, for instance, in $\text{SrCoO}_{3-\delta}/\text{YSZ}$ and VO_x/YSZ heterostructures,^{27,28} voltage-controlled oxygen diffusion can induce electrochemically triggered phase transition at temperatures above 300°C . It is remarkable that in the present work the property changes are observed while applying voltage at room temperature, without the need of any heat treatment. Figure 1(b) also reveals that magnetic recovery (i.e., the disappearance of MOKE signal) can be achieved by applying an opposite (i.e., positive) gate voltage.

Fluorescence yield Co $L_{2,3}$ -edge XAS and XMCD spectra—the latter is calculated as the difference between the XAS spectra measured with left and right circularly polarized photons (μ^- and μ^+ , respectively)—for the as-grown, treated, and recovered CoO_x/YSZ structures are shown in Fig. 1(c). Note that the XAS recorded in total electron yield mode, which is more surface sensitive and probes only approximately a 5 nm top layer, shows no observable changes in the spectra of the as-grown and treated samples (see supplementary material S3), implying that the modification of electronic structure may take place at the CoO_x/YSZ interface region. The difference in absorption spectral shapes is negligible in the XAS recorded with the opposite helicities for the as-grown sample, correlating with the predominant paramagnetic behavior of the as-grown CoO_x . It is worth noting that the XMCD spectrum, though, reveals traces of a weak ferromagnetic contribution. This small ferromagnetic signal is common in sputtered cobalt oxide films,^{29,30} and can be attributed to a small fraction of residual Co clusters that do not become fully oxidized during the sputtering process and/or the formation of a weak ferromagnetic order at the CoO/ Co_3O_4 interface (i.e., uncompensated spins).³¹ However, after gating, a clear discrepancy between the μ^+ and μ^- polarized XAS spectra becomes visible near the L_3 edge (at photon energy of around 778 eV). The main L_3 (L_2) peak shows more (less) intensity in the spectrum for μ^- polarization compared with μ^+ polarization. Consequently, there is an important intensity increase at both L_3 (negative peak) and L_2 (positive peak) edges in the XMCD profile, and, therefore, an increment in magnetic moment, for the gated sample. This is consistent with the observed ferromagnetism generation upon voltage actuation in the MOKE study. The reversible changes of the XAS intensity and XMCD signals, as shown in Fig. 1(c), constitute another clear evidence for the room-temperature ON–OFF switching of the ferromagnetic states. In fact, room-temperature voltage-driven transportation of O^{2-} species through oxygen vacancies in the YSZ film was reportedly responsible for the reversible, nonvolatile multi-level conductance states in the WO_3/YSZ system, rendering interesting neuromorphic functionalities using relatively low voltages.³² Another interesting reported effect is the resistive switching in $\text{Pr}_{1-x}\text{Ca}_x\text{MnO}_3/\text{YSZ}$ heterostructures due to the application of positive biases, which induces O^{2-}

migration from $\text{Pr}_{1-x}\text{Ca}_x\text{MnO}_3$ to the tunnel YSZ layer.³³ It should be pointed out that in previous studies on magneto-ionics using a liquid electrolyte and relatively thick Co_3O_4 layers (of the order of 100–200 nm), voltage actuation times of the order of 30 min or longer were required to induce significant changes in the induced magnetization.^{10,29} Here magneto-ionics effects are much faster. This can be due to the employed lower thickness of CoO_x , which accelerates magneto-ionics,²⁹ or the presence of the top Pt capping layer. Indeed, recent studies have shown that noble metals can induce fast interfacial oxygen migration due to the weakening of the metal–oxygen bond in some transition metal perovskite oxides.³⁴ Also interesting is that the recovery time (80 s) is much longer than the time needed to trigger magneto-ionics (10 s). This can be due to a combination of factors. First, if oxygen ions diffuse long distances from their initial position, it might be difficult to bring them back to their original location. If they remain in other parts of the sample (forming, e.g., Co_3O_4 clusters), they will not necessarily move back easily to reoxidize ferromagnetic Co clusters. However, YSZ might be more prone to oxygen than CoO_x , which makes the reverse oxygen ion transport more difficult. Finally, an additional factor could be, as observed in some other materials such as SrCoO_x , that there could be simultaneous oxidation and reduction of Co due to the motion of oxygen ions and protons.^{35,36}

To further investigate the OFF–ON switching of ferromagnetism, Fig. 2(a) illustrates the MOKE hysteresis loops recorded *ex situ* on the CoO_x/YSZ heterostructures gated under $V_G = -5$ V for different actuation times, t_G . A ferromagnetic-like hysteresis loop develops already at $t_G = 5$ s, indicating the onset of magneto-ionics in this system. Remarkably, the MOKE loops become wider and the Kerr amplitude increases when increasing the gating duration. As shown in the evolution of coercivity (H_C) and squareness ratio (M_R/M_S) as a function of t_G [see Fig. 2(b)], both H_C and M_R/M_S experience a significant rise during the first 10 s, and then they grow at a slower rate up to 50 s, where they eventually tend to level off. More specifically, H_C rapidly increases up to 11.2 Oe within the first 10 s of voltage actuation, giving rise to an increased rate of 1.1 Oe/s. By increasing t_G up to 50 s, H_C further increases to 29.0 Oe, representing a reduced average rate of 0.6 Oe/s in this period. A similar trend is observed in the variation of M_R/M_S . The changes in H_C and M_R/M_S continue with t_G and approach 34.7 Oe and 0.75, respectively, for the maximum t_G used in our experiments (100 s). A similar behavior is also observed in the amplitude of the Kerr signal evolution, as seen from the inset of Fig. 2(b). From these observations, it can be speculated that in the first stages of voltage application, small (ferromagnetic) cobalt clusters are formed, which tend to grow in size upon sustained gating. This causes an increase in magnetic anisotropy and a reduced influence of thermal agitation effects, resulting in larger H_C and M_R/M_S values. The monotonic increase in coercivity with biasing duration suggests that the generated ferromagnetic counterparts are probably rather isolated, with limited exchange/dipolar interactions among clusters which would be detrimental to coercivity.

Finally, we also observed a strong dependence of the hysteresis behavior on the magnitude of the applied gate voltage, as shown in Fig. 3(a). Ferromagnetic-like hysteretic behavior with appreciable M_S emerges under a gate voltage of -1 V. Above this threshold voltage, the ferromagnetic response becomes more and more pronounced, i.e., the squareness ratio gets gradually larger, with increasing magnitude of the gate voltage, indicating progressive reduction of the CoO_x

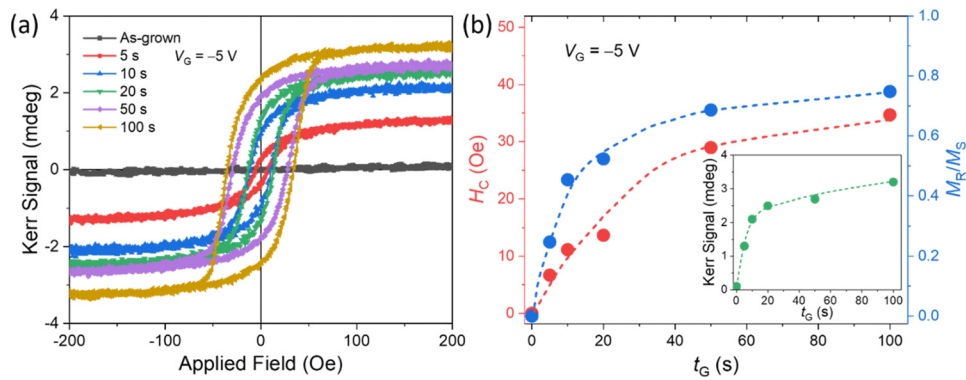


FIG. 2. (a) MOKE hysteresis loops for the CoO_x/YSZ heterostructures after gating under $V_G = -5\text{ V}$ for various times. (b) Dependence of coercivity (H_C) and squareness ratio (M_R/M_S) on gating duration (t_G). Red and blue circles are data points, and the dashed lines are drawn as a guide to the eye. The inset in (b) shows the magnitude of the Kerr signal under an applied in-plane magnetic field of 200 Oe.

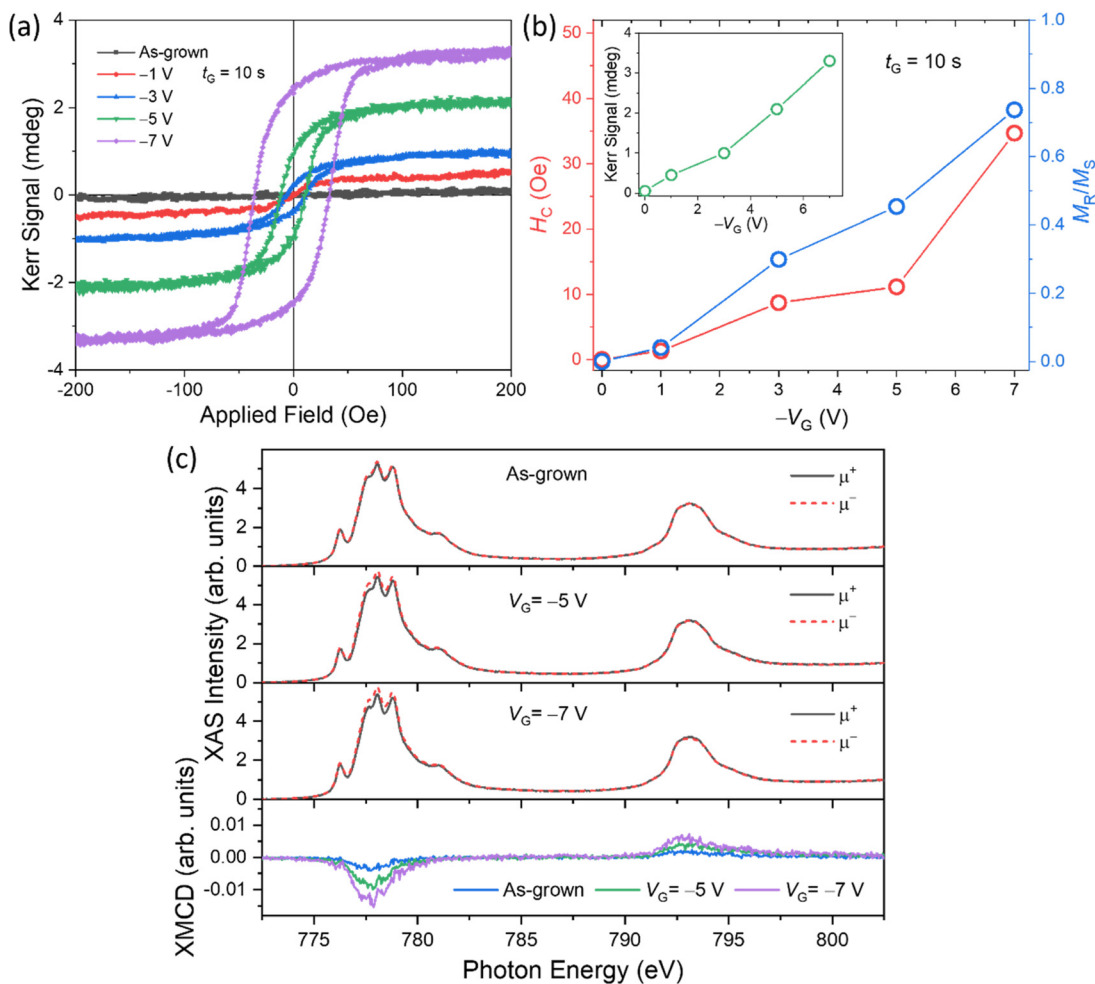


FIG. 3. (a) MOKE hysteresis loops for the CoO_x/YSZ heterostructures after gating under different voltages for a duration $t_G = 10\text{ s}$. (b) Dependence of coercivity (H_C) and squareness ratio (M_R/M_S) on the magnitude of gating voltages, obtained from panel (a). Red and blue open circles are data points, and the solid lines are guides to the eye. The inset in (b) shows the magnitude of the Kerr signal under an in-plane applied field of 200 Oe. (c) $\text{Co } L_{2,3}$ -edge XAS and XMCD spectra for the as-grown and treated (under different V_G) CoO_x/YSZ structures. Absorption spectra of right (μ^+) and left (μ^-) circularly polarized x rays are depicted in dashed red and black solid lines, respectively.

layer due to voltage-driven electrochemistry processes. As plotted in Fig. 3(b), the values of H_C and M_R/M_S increase continuously from zero for $V_G = 0$ V to 34.7 Oe and 0.74, respectively, after gating under $V_G = -7$ V for 10 s. This correlates with the monotonic increase in Kerr signal. Co $L_{2,3}$ -edge XAS and XMCD spectra for the as-grown and treated (under different V_G) CoO_x/YSZ structures are shown in Fig. 3(c). After gating, while no significant changes in voltage-dependent average XAS spectra are observed (probably due to the relatively large beam spot size, $\sim 100 \mu\text{m}^2$),³³ the generation of the XMCD signal, therefore the magnetic moment, becomes visible. Note that the XMCD spectra change their signs when the direction of the applied magnetic field is reversed (not shown), confirming that the observed XMCD signals are of magnetic origin. The observed changes in the absorption spectral shape and the progressive enhancement of the XMCD signal are consistent with the MOKE results, confirming magneto-ionic switching from non-magnetic to ferromagnetic state in CoO_x/YSZ heterostructures upon electrolyte gating.

In summary, we have experimentally demonstrated electrical control of magnetization in the relatively thick CoO_x/YSZ solid-state system at room temperature, using magneto-ionic gating. The electrochemical reduction of CoO_x due to the application of negative gate voltages, associated with oxygen ion migration toward the ionic conducting YSZ layer, leads to the generation of magnetization and the occurrence of ferromagnetic hysteresis behavior. Both the coercivity and squareness ratio of the hysteresis loops increase with increasing the magnitude of the applied voltage and/or the gating duration (up to a certain saturation value). These trends are presumably related to the formation of small (ferromagnetic) cobalt clusters in the first stages of voltage application, which tend to grow in size upon sustained gating. The monotonic increase in coercivity with biasing duration suggests that the generated ferromagnetic counterparts are rather isolated, without pronounced exchange or dipolar interactions among clusters that would be detrimental to coercivity. These effects can be attributed to voltage-driven O^{2-} ion motion across the CoO_x/YSZ interface. This study reveals oxygen migration in all-solid-state magneto-ionic systems based on Si-compatible YSZ, an oxide that is widely employed in oxygen sensors or as an electrolyte for solid oxide fuel cells due to its high ion conductivity.

See the [supplementary material](#) for x-ray diffraction θ - 2θ scan of YSZ/Si(001), XAS spectra of as-grown cobalt oxide and reference samples, and XAS studies of the as-grown, treated, and recovered CoO_x/YSZ structures.

Financial support by the European Union's Horizon 2020 Research and Innovation Programme (BeMAGIC European Training Network, ETN/ITN Marie Skłodowska-Curie Grant No. 861145), the European Research Council (2021-ERC-Advanced REMINDS Grant No. 101054687), the Generalitat de Catalunya (Nos. 2021-SGR-00651 and 2021 SGR 00804), and the Spanish Government (Nos. PID2020-112548RB-I00, PID2020-116844RB-C21, PDC2021-121276-C31, PID2019-107727RB-I00, PID2023-147211OB-C21, TED2021-130453B-C21, and TED2021-130453B-C22, and the MCIN/AEI/10.13039/501100011033 and "European Union NextGenerationEU/PRTR" Grant No. CNS2022-135230) are acknowledged. The XAS/XMCD experiments were performed at BL29-BOREAS beamline at ALBA Synchrotron with the collaboration of ALBA staff. E.M. is a Serra Hünter Fellow.

AUTHOR DECLARATIONS

Conflict of Interest

The authors have no conflicts to disclose.

Author Contributions

Zheng Ma: Conceptualization (equal); Data curation (equal); Formal analysis (equal); Investigation (equal); Writing – original draft (equal); Writing – review & editing (equal). **Zhengwei Tan:** Formal analysis (equal); Investigation (equal); Methodology (equal). **Alberto Quintana:** Conceptualization (equal); Formal analysis (equal); Investigation (equal); Methodology (equal). **Irena Spasojevic:** Formal analysis (equal); Resources (equal). **Nicolau López-Pintó:** Formal analysis (equal); Validation (equal). **Florencio Sanchez:** Conceptualization (equal); Methodology (equal); Resources (equal); Writing – review & editing (equal). **Ignasi Fina:** Conceptualization (equal); Methodology (equal); Resources (equal); Writing – review & editing (equal). **Javier Herrero-Martin:** Formal analysis (equal); Methodology (equal); Resources (equal); Software (equal); Validation (equal). **Enric Menendez:** Conceptualization (equal); Funding acquisition (equal); Methodology (equal); Supervision (equal); Validation (equal); Writing – review & editing (equal). **Jordi Sort:** Conceptualization (equal); Funding acquisition (equal); Methodology (equal); Project administration (equal); Supervision (equal); Validation (equal); Writing – review & editing (equal).

DATA AVAILABILITY

The data that support the findings of this study are available from the corresponding authors upon reasonable request.

REFERENCES

- Q. Wang, Y. Gu, C. Chen, F. Pan, and C. Song, *J. Phys. Chem. Lett.* **13**, 10065 (2022).
- J. de Rojas, A. Quintana, G. Rius, C. Stefani, N. Domingo, J. L. Costa-Krämer, E. Menéndez, and J. Sort, *Appl. Phys. Lett.* **120**, 070501 (2022).
- A. Molinari, H. Hahn, and R. Kruk, *Adv. Mater.* **30**, 1703908 (2018).
- C. Navarro-Senent, A. Quintana, E. Menéndez, E. Pellicer, and J. Sort, *APL Mater.* **7**, 030701 (2019).
- H. Ekawa, J. Shen, K. Toyoki, R. Nakatani, and Y. Shiratsuchi, *Appl. Phys. Lett.* **122**, 062404 (2023).
- M. Ameziane, J. Huhtasalo, L. Flajsman, R. Mansell, and S. van Dijken, *Nano Lett.* **23**, 3167 (2023).
- L. Herrera Diez, Y. T. Liu, D. A. Gilbert, M. Belmeguenai, J. Vogel, S. Pizzini, E. Martinez, A. Lamperti, J. B. Mohammedi, A. Laborieux, Y. Roussigné, A. J. Grutter, E. Arenholtz, P. Quarterman, B. Maranville, S. Ono, M. Salah El Hadri, R. Tolley, E. E. Fullerton, L. Sanchez-Tejerina, A. Stashkevich, S. M. Chérif, A. D. Kent, D. Querlioz, J. Langer, B. Ocker, and D. Ravelosona, *Phys. Rev. Appl.* **12**, 034005 (2019).
- D. A. Gilbert, A. J. Grutter, E. Arenholz, K. Liu, B. J. Kirby, J. A. Borchers, and B. B. Maranville, *Nat. Commun.* **7**, 12264 (2016).
- S. Dasgupta, B. Das, M. Knapp, R. A. Brand, H. Ehrenberg, R. Kruk, and H. Hahn, *Adv. Mater.* **26**, 4639 (2014).
- A. Quintana, E. Menéndez, M. O. Liedke, M. Butterling, A. Wagner, V. Sireus, P. Torruella, S. Estradé, F. Peiró, J. Dendooven, C. Detavernier, P. D. Murray, D. A. Gilbert, K. Liu, E. Pellicer, J. Nogues, and J. Sort, *ACS Nano* **12**, 10291 (2018).
- M. Cialone, A. Nicolenco, S. Robbenolt, E. Menéndez, G. Rius, and J. Sort, *Adv. Mater. Interfaces* **8**, 2001143 (2021).
- J. de Rojas, A. Quintana, A. Lopeandía, J. Salguero, B. Muñoz, F. Ibrahim, M. Chshiev, A. Nicolenco, M. O. Liedke, M. Butterling, A. Wagner, V. Sireus,

- L. Abad, C. J. Jensen, K. Liu, J. Nogués, J. L. Costa-Krämer, E. Menéndez, and J. Sort, *Nat. Commun.* **11**, 5871 (2020).
- ¹³Z. Ma, L. Fuentes-Rodríguez, Z. Tan, E. Pellicer, L. Abad, J. Herrero-Martín, E. Menéndez, N. Casañ-Pastor, and J. Sort, *Nat. Commun.* **14**, 6486 (2023).
- ¹⁴M. Jaipal and A. Chatterjee, *J. Phys. Chem. C* **121**, 14534 (2017).
- ¹⁵A. Bogicevic and C. Wolverton, *Phys. Rev. B* **67**, 024106 (2003).
- ¹⁶A. Chroneos, B. Yildiz, A. Tarancón, D. Parfitta, and J. A. Kilner, *Energy Environ. Sci.* **4**, 2774 (2011).
- ¹⁷K.-Y. Lee, S. Jo, A. J. Tan, M. Huang, D. Choi, J. H. Park, H.-I. Ji, J.-W. Son, J. Chang, G. S. D. Beach, and S. Woo, *Nano Lett.* **20**, 3435 (2020).
- ¹⁸R. Mishra, D. Kumar, and H. Yang, *Phys. Rev. Appl.* **11**, 054065 (2019).
- ¹⁹Z. Tan, J. de Rojas, S. Martins, A. Lopeandia, A. Quintana, M. Cialone, J. Herrero-Martín, J. Meersschat, A. Vantomme, J. L. Costa-Krämer, J. Sort, and E. Menéndez, *Mater. Horiz.* **10**, 88 (2023).
- ²⁰P. Monalisha, Z. Ma, E. Pellicer, E. Menéndez, and J. Sort, *Adv. Electron. Mater.* **9**, 2300249 (2023).
- ²¹J. C. Delgado, F. Sánchez, R. Aguiar, Y. Maniette, C. Ferrater, and M. Varela, *Appl. Phys. Lett.* **68**, 1048 (1996).
- ²²P. de Coux, R. Bachelet, C. Gatel, B. Warot-Fonrose, J. Fontcuberta, and F. Sánchez, *CrystEngComm* **14**, 7851 (2012).
- ²³M. Scigaj, N. Dix, I. Fina, R. Bachelet, B. Warot-Fonrose, J. Fontcuberta, and F. Sánchez, *Appl. Phys. Lett.* **102**, 112905 (2013).
- ²⁴A. Barla, J. Nicolás, D. Cocco, S. M. Valvidares, J. Herrero-Martín, P. Gargiani, J. Moldes, C. Ruget, E. Pellegrin, and S. Ferrer, *J. Synchrotron Rad.* **23**, 1507 (2016).
- ²⁵I. Garbayo, F. Chiabrera, N. Alayo, J. Santiso, A. Morata, and A. Tarancón, *J. Mater. Chem. A* **7**, 25772 (2019).
- ²⁶I. Garbayo, A. Tarancón, J. Santiso, F. Peiró, E. Alarcón-LLadó, A. Cavallaro, I. Gràcia, C. Cané, and N. Sabaté, *Solid State Ionics* **181**, 322 (2010).
- ²⁷Q. Lu, S. R. Bishop, D. Lee, S. Lee, H. Bluhm, H. L. Tuller, H. N. Lee, and B. Yildiz, *Adv. Funct. Mater.* **28**, 1803024 (2018).
- ²⁸Q. Lu and B. Yildiz, *Nano Lett.* **16**, 1186 (2016).
- ²⁹S. Martins, J. de Rojas, Z. Tan, M. Cialone, A. Lopeandia, J. Herrero-Martín, J. L. Costa-Krämer, E. Menéndez, and J. Sort, *Nanoscale* **14**, 842 (2022).
- ³⁰Z. Tan, Z. Ma, L. Fuentes, M. O. Liedke, M. Butterling, A. G. Attallah, E. Hirschmann, A. Wagner, L. Abad, N. Casañ-Pastor, A. F. Lopeandia, E. Menéndez, and J. Sort, *ACS Nano* **17**, 6973 (2023).
- ³¹N. Fontañá-Troitiño, S. Liébana-Viñas, B. Rodríguez-González, Z.-A. Li, M. Spasova, M. Farle, and V. Salgueiriño, *Nano Lett.* **14**, 640 (2014).
- ³²R. D. Nikam, M. Kwak, and H. Hwang, *Adv. Electron. Mater.* **7**, 2100142 (2021).
- ³³C. Baeumer, T. Heisig, B. Arndt, K. Skaja, F. Borgatti, F. Offi, F. Motti, G. Panaccione, R. Waser, S. Menzel, and R. Dittmann, *Faraday Discuss.* **213**, 215 (2019).
- ³⁴Q. Wang, Y. Gu, W. Zhu, L. Han, F. Pan, and C. Song, "Noble-Metal-Assisted fast interfacial oxygen migration with topotactic phase transition in perovskite oxides," *Adv. Funct. Mater.* **31**(50), 2106765 (2021).
- ³⁵Q. Wang, Y. Gu, C. Chen, L. Qiao, F. Pan, and C. Song, *ACS Appl. Mater. Interfaces* **15**, 1574 (2023).
- ³⁶S. Lu, F. Yin, Y. Wang, N. Lu, L. Gao, H. Peng, Y. Lyu, Y. Long, J. Li, and P. Yu, "Facile pathways to synthesize perovskite strontium cobalt oxides," *Adv. Funct. Mater.* **33**(2), 2210377 (2023).